fluids

MDPI

Article

Effects of Permeability and Gravity on Capillary Imbibition in Filter Paper

Josefina Janeth Miranda-Blancas [1], José Martínez-Trinidad [1,*], Abraham Medina-Ovando [2], Luis Alfonso Moreno-Pacheco [1], Fernando Alonso-Cruz [1], Osvaldo Quintana-Hernández [1] and Ricardo Andrés García-León [3,*]

[1] Grupo Ingeniería de Superficies, SEPI-ESIME Zacatenco, Instituto Politécnico Nacional, Mexico City C.P. 07738, Mexico; lamoreno@ipn.mx (L.A.M.-P.)
[2] SEPI-ESIME Azcapotzalco, Instituto Politécnico Nacional, Mexico City C.P. 02460, Mexico
[3] Grupo de investigación INGAP, Facultad de Ingeniería, Universidad Francisco de Paula Santander Ocaña, Ocaña C.P. 546552, Colombia
* Correspondence: jomartinezt@ipn.mx (J.M.-T.); ragarcial@ufpso.edu.co (R.A.G.-L.)

Highlights

- Imbibition front position is governed by the permeability of the porous medium.
- At an inclination of 80°, circular imbibition fronts exhibit displacement in the di-rection of gravity.
- The temporal exponent for imbibition remains consistently below 0.5.
- Experimental results deviate from the scaling predicted by the Washburn model.

Abstract

Capillary imbibition is the process by which liquids are absorbed into porous materials as a result of capillary pressure differences at the pore scale. Accurate characterization of imbibition dynamics, particularly in the presence of gravitational potential, is essential for understanding fluid transport in diverse systems such as soil, fractured rocks, filtration media, and plant roots. This study presents systematic imbibition experiments using filter papers with pore sizes of 2.5 μm, 11 μm, and 20 μm, each inclined at 80° to quantify the influence of gravitational potential on imbibition behavior. For horizontally positioned samples, the imbibition front propagated radially and symmetrically, exhibiting a power law dependence on time. The measured temporal exponents ranged from 0.386 to 0.403, consistently lower than the theoretical value of 1/2 predicted by the Lucas–Washburn law. With increasing permeability, the temporal exponent approached the Washburn limit, indicating a marked dependence of imbibition dynamics on pore structure. For the inclined configuration at an 80° angle, the imbibition fronts remained nearly circular but exhibited a pronounced displacement of the front center toward gravity. This displacement increased with permeability, from approximately 0.497 cm for the 11 μm filter paper to 3545 cm for the 20 μm filter paper, highlighting the combined effects of permeability and gravitational potential on fluid movement. Furthermore, the advance of the imbibition front was significantly slower in the smallest pores (2.5 μm) compared to the larger ones. Experimental results were evaluated against a theoretical model proposed by Medina, demonstrating moderate quantitative agreement at early times, when gravitational potential effects are less significant. These findings confirm that both the temporal scaling exponent and the spatial evolution of the imbibition front are governed by the porous medium's permeability and inclination angle, providing experimental evidence of deviations from ideal Washburn behavior in real porous systems.

Check for updates

Academic Editor: Akira Nakayama

Received: 22 April 2026
Revised: 15 May 2026
Accepted: 17 May 2026
Published: 21 May 2026

Copyright: © 2026 by the authors. Licensee MDPI, Basel, Switzerland. This article is an open access article distributed under the terms and conditions of the Creative Commons Attribution (CC BY) license.

Keywords: porous media; capillary imbibition; Washburn law; influence of gravitational potential on imbibition; permeability; Darcy's equation

1. Introduction

1.1. General Concepts

Instantaneous capillary imbibition is an interfacial phenomenon in which a porous medium comes into contact with a fluid and spontaneously absorbs it. This process is governed exclusively by capillary forces, so the fluid advance is driven by pressure differences between the invading fluid and the surrounding medium. These pressure differences are determined by the product of the surface tension and the interface curvature, as described by the Young–Laplace equation for capillary systems [1]. During the initial stages of imbibition, inertial and gravitational effects are generally negligible, enabling the advancement of the fluid front to be described solely by capillary and viscous forces.

A porous medium is defined as a material characterized by a network of interconnected pores, voids, or fibers that facilitate fluid transport throughout its structure. Examples include minerals, rocks, geological formations, biological tissues, polymers, food products, and filter paper. Owing to the prevalence of capillary imbibition in such materials, this phenomenon has been extensively investigated for its significance in both natural and technological processes, including seed germination, paper manufacturing, biomedical applications, filtration systems, and oil recovery from porous rocks [2]. Therefore, given its predominant presence, studying it is imperative to establish equations that define its behavior. This work does not have immediate engineering applications because the experiments were conducted under controlled flow conditions. However, important factors to consider in understanding imbibition behavior include the medium's permeability and the gravitational potential. The particular interest of this experimental work is the analysis of water flow through filter paper with different permeabilities, as well as the effects of gravitational potential.

A foundational theoretical framework for capillary imbibition was established by Washburn in 1921 [3]. The Washburn model analyzes fluid advancement in both horizontal and vertical capillaries and shows that the penetration length l depends on parameters such as capillary radius r, surface tension γ, contact angle θ, and dynamic viscosity, as summarized in Equation (1). In this formulation, μ denotes the dynamic viscosity of the fluid. The model predicts that the advancement of the imbibition front follows a diffusive scaling law, with penetration length proportional to the square root of time (i.e., $l \sim t^{1/2}$). This relationship, known as the Lucas–Washburn law, forms the basis for understanding capillary-driven transport in ideal porous media and serves as a benchmark for interpreting deviations observed in real systems, where parameters such as permeability, tortuosity, and gravity significantly affect imbibition dynamics.

$$l^2 = \left(\frac{\gamma}{\mu}\frac{\cos(\theta)}{2}\right)rt. \quad (1)$$

1.2. Related Studies

Numerous investigations have extended the classical Washburn model to describe capillary imbibition in porous media, often conceptualized as networks of interconnected capillaries. Considerable research has focused on quantifying the maximum imbibition height of a fluid in various porous structures. For example, Agihtias (2022) [4] examined fluid rise in capillaries under diverse conditions, such as varying gravitational fields, surface roughness with fractal properties, different pore sizes, and dynamic viscosities.

This work introduced a theoretical framework for estimating the maximum imbibition height and provided experimental evidence that the observed height in a single capillary is markedly lower than predictions from the Lucas–Washburn model. Likewise, Fries and Dreyer (2008) [5] accounted for the influence of surface roughness and effective viscosity in their theoretical approach, offering further insight into deviations from classical theory.

Multiple studies have refined the Washburn equation to better represent the structural complexity of porous media, with particular emphasis on the effect of tortuosity. Cai (2006) [6] conducted imbibition experiments in randomly ordered fibrous porous materials, demonstrating that tortuosity significantly impacts the temporal exponent in Washburn-type relations. The resulting exponent was found to scale as ~$1/(2D_T)$, where D_T value is governed by the tortuosity of the medium and yielding values consistently lower than 1/2. Additional support for the non-universality of the Washburn equation was provided by Chang S. (2020) [7], who conducted different imbibition experiments on filter paper, accounting for thickness changes before and after wetting, and supplemented the analysis with a numerical model. Similarly, Patari (2020) [8] used capillary imbibition in filter paper to monitor milk penetration and assess dilution with water.

Cummins et al. (2017) [9] conducted experimental studies on fluid dynamics in porous media using filter papers with 10 different pore sizes, generating time-dependent imbibition data over a broad range of permeabilities. In addition to investigations of maximum imbibition height, multiple studies have explored horizontal imbibition in planar geometries. For example, Chang et al. (2018) [10] examined one-dimensional horizontal imbibition in various grades of Whatman filter paper and observed that the Washburn model consistently overestimates experimentally measured imbibition. Notably, agreement between theoretical predictions and experimental results was limited to the initial imbibition phase, typically within the first 7 s.

The influence of gravity on imbibition has also been explored using numerical approaches. El-Amin and Shuyu Sun (2011) [11] conducted two-dimensional numerical simulations incorporating gravitational potential effects and demonstrated that, under zero-gravity conditions, the flow is uniform and can be effectively described as one-dimensional. In contrast, nonzero gravity leads to nonuniform flow patterns, requiring a fully two-dimensional description.

The development of paper-based analytical devices (μPADs) has revolutionized point-of-care diagnostics due to their low cost and autonomy. However, precise control of fluid transport remains a challenge because it relies solely on spontaneous imbibition. Ting Cheng et al. [12] review the design, fabrication, and applications of multi-dimensional microfluidic paper-based analytical devices (μPADs) for noninvasive health diagnostics. Gharagozlou et al. (2024) [13] present a theoretical extension of the Richards equation to model the spontaneous imbibition of yield stress fluids, such as blood, in paper-based diagnostic kits.

The study of fluid transport in porous matrices is not only fundamental to paper-based microfluidics but also represents a cornerstone in large-scale industrial applications. For example, rock permeability and water absorption in pores are complex problems that reservoir science and enhanced oil recovery (EOR) methods must constantly address. The Eocene limestones found in the Balkassar oil field, Pakistan, exhibit porosities ranging from macropores (>100 μm) to micropores (<20 μm). Shah (2026) [14] conducted a series of thermo-mechanical tests to assess how the rock's integrity and flow capacity are modified. The results showed that these tests increased rock permeability, indicating that thermo-mechanical processes can enhance fluid movement through limestone pores.

Understanding flow mechanisms is crucial for assessing the effectiveness of fracturing, where backflow data and pressure transient tests are used to interpret the connectivity of

the porous network. Han et al. (2025) [15] investigated the flowback and CO_2 sequestration behavior. Among their key findings, which observed that the fracturing fluid is primarily retained in small pores, the authors determined that increasing the soaking time reduces flowback efficiency (due to imbibition driven by capillary forces). The study focuses on tight gas reservoirs, defined by their ultra-low permeability, which impedes gas flow.

On the other hand, recent advances have integrated machine learning (ML) techniques to manage the complexity of the phenomenon and also effectively select enhanced oil recovery (EOR) methods, emphasizing the need for precise physical parameters to improve predictive models. For an ML algorithm to learn to predict the phenomenon, real experimental data is needed. Madhumaya et al. (2026) [16] present a novel approach to predicting oil recovery in laboratory experiments using artificial intelligence. Their research proposes a Time Series Machine Learning (TSML) framework for forecasting cumulative oil recovery (EOR) using polymers. Their aim is to offer a lighter, faster tool than conventional reservoir simulators, which require detailed, costly rock characterization and simulation.

Medina (2024) [17] recently developed a theoretical framework for imbibition in planar porous media, considering two configurations: a horizontal plane and a plane inclined at an angle $\alpha = \pi/2$ with respect to the horizontal. In this model, the fluid source is a capillary of radius r_0, and after a short time δt, a wetted surface develops. By solving the Laplace equation in conjunction with Darcy's law, it was demonstrated that the fluid front advances as the square root of time. For inclined planes, the analysis focuses on short-time behavior, where the imbibition fronts in both setups are described by Equation (2). In this context, ϕ represents a constant volumetric flow rate and D the thickness of the porous medium. Under these assumptions, the imbibition fronts expand radially, and the dynamics follow a Washburn-type scaling.

$$r_s = \sqrt{\frac{\phi t}{\pi D}} \tag{2}$$

1.3. Aim of This Work

This study aims to experimentally investigate capillary imbibition in two-dimensional, planar porous media, focusing on quantifying the effects of gravity and permeability on the evolution of the imbibition front. In contrast to previous works, which typically consider imbibition as a one-dimensional process initiated along a single direction, this investigation examines imbibition on an inclined plane using filter paper as the model porous medium. The sheets are inclined at a fixed angle, and fluid advancement is measured along four radial directions from the imbibition point, enabling comprehensive characterization of both the shape and displacement of the imbibition front in response to gravity.

To isolate the effects of gravity and porous structure, key fluid properties, including density, dynamic viscosity, and surface tension, were maintained constant throughout the experiments, while permeability is systematically varied by using filter papers with different pore sizes. This methodology enables direct evaluation of how pore size and permeability influence both the dynamics and geometry of the imbibition front. The experimental results are then compared with theoretical predictions reported by Medina (2024) [17], specifically those derived from Equation (2), which incorporates gravitational effects under analogous assumptions and parameter constraints. This comparison facilitates the assessment of the validity and limitations of the theoretical model for short-time imbibition in inclined porous planes.

Unlike traditional studies that focus on horizontal imbibition, this work provides a comprehensive statistical analysis of directional flow under gravitational influence. By analyzing the transition of temporal exponents in inclined cellulose matrices, we reveal how the competition between capillary suction and gravity becomes significant as a function of pore architecture. Also, this study addresses a critical gap in the literature by providing

a systematic characterization of three commercial cellulose architectures (2.5, 11, and 20 μm). The novelty lies in establishing a predictive framework that correlates pore scale morphology with macroscopic wetting kinetics, thereby providing essential design parameters to ensure reliable, reproducible fluid transport in paper-based sensors. And the experimental dataset presented in this study provides a solid foundation for its future integration into machine learning (ML) frameworks.

2. Materials and Methods

Figure 1 presents the methodological workflow implemented to assess the influence of permeability and gravity force on capillary imbibition in filter paper. The experimental setup was designed to control the inclination angle of the filter paper sheet while ensuring capillary-driven liquid transport that occurred without external forces.

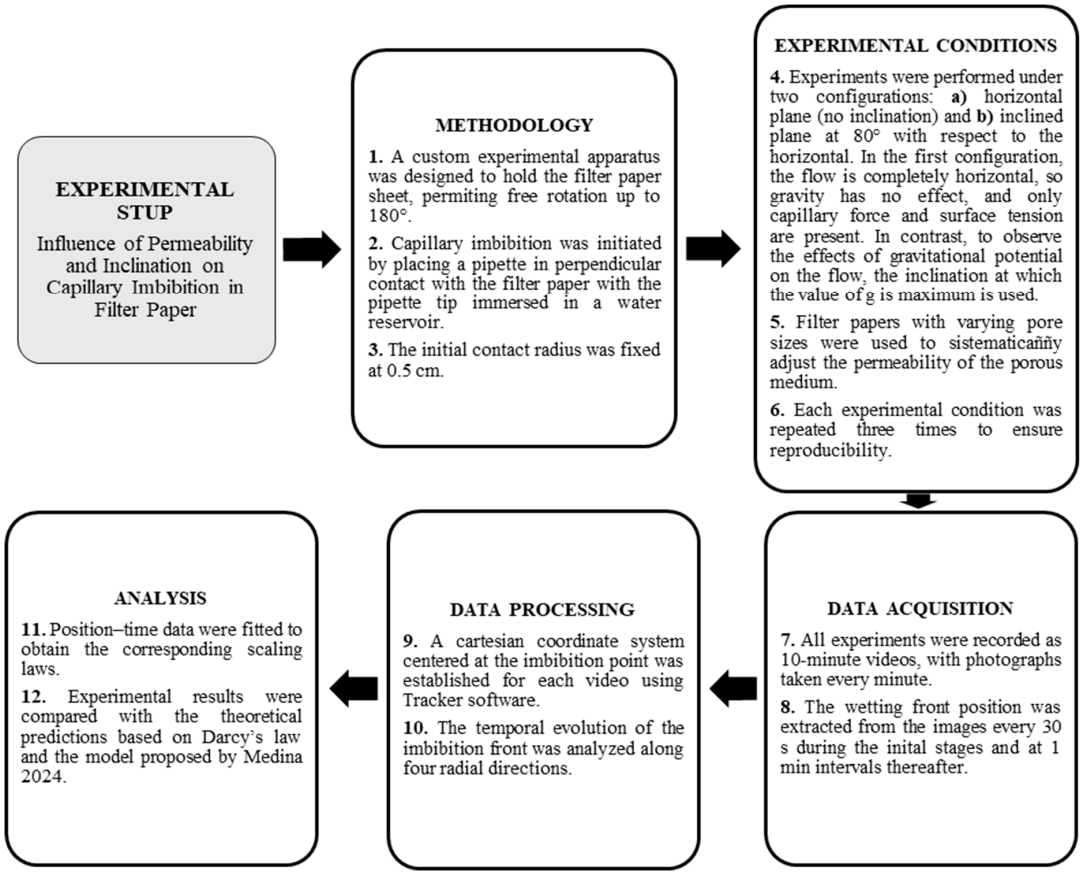


Figure 1. Schematic representation of the experimental methodology.

A custom apparatus was constructed to permit the adjustment of the filter paper's inclination relative to the horizontal plane, guaranteeing that liquid movement was governed exclusively by capillary forces. Experiments were initially conducted with the paper in a horizontal configuration, followed by tests at an inclination angle of 80°, enabling direct comparisons of imbibition dynamics under varying gravitational components. The experiments were conducted at 80° to allow for a direct and rigorous comparison with the analytical framework established by Medina [17]. The equation governing the critical time (Equation (8)) involves a dependence of cos (θ) that approaches an asymptotic limit as θ approaches 90°, which can lead to numerical instability in that specific theoretical model. To ensure a stable and valid comparison between our experimental data and existing theory, 80° was chosen as the representative tilt angle at which the gravitational effect is maximal. For each pore size, at least 3 repetitions were performed to ensure experimental

reproducibility. Each test was recorded for 10 min using a video camera, starting 50 min after imbibition to capture steady, well-defined capillary fronts. The resulting videos and images were analyzed using Image Tracker software V.2.1 to measure the imbibition front position at 30 s intervals.

Subsequently, the experimental data were processed and analyzed using tables, graphs, and comparative discussions to evaluate the effects of permeability and inclination on imbibition behavior. This methodology provides a systematic framework for quantifying capillary transport under controlled geometric and material conditions, ensuring consistent, reliable results.

2.1. Sample Details

To ensure that the imbibition process is governed exclusively by capillary forces, a straw with an internal radius of r = 3 mm, filled with cotton, was employed as the fluid conduit. One end of the straw was immersed in a water reservoir, allowing the pressure gradient and capillary action to drive water transport upward through the straw. The opposite end was placed in contact with the filter paper sheet at a right angle, thereby initiating imbibition within the porous medium. Under this configuration, fluid supply is regulated solely by capillary pressure, with no additional external forces affecting fluid advancement on the filter paper surface. As a result, the wetting process is controlled by the intrinsic properties of the fluid and the porous substrate, as schematically depicted in Figure 2.

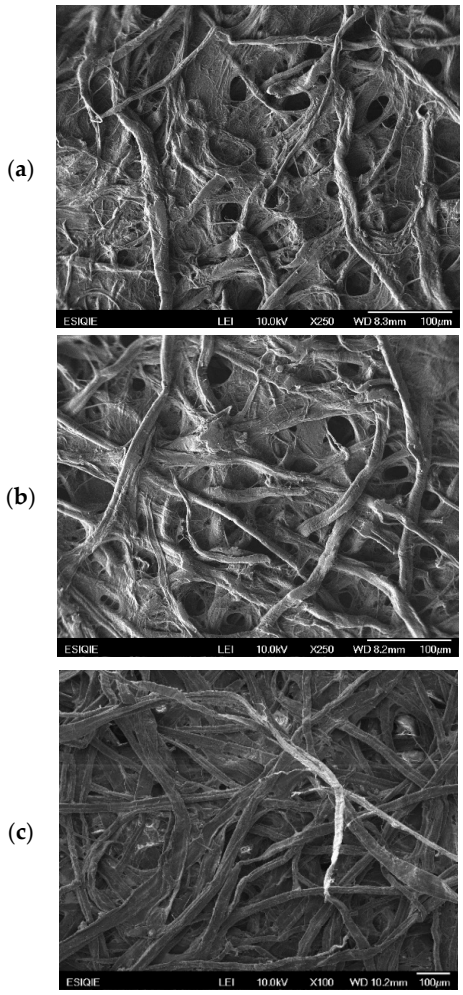


Figure 2. Micrographs made with a field emission scanning electron microscope (FESEM). (**a**) Whatman filter paper, 2.5 µm pore size (250×); (**b**) Whatman filter paper, 11 µm pore size (250×);

and (**c**) Nacional filter paper, 20 µm pore size (100×). The stochastic distribution of cellulose fibers and the variation in pore connectivity are observed factors that determine the anisotropy in the system's microfluid dynamics.

A custom device was constructed consisting of a square wooden frame (25 cm × 25 cm) used to hold the 2.5 µm and 11 µm Whatman filter papers, which were used to achieve the experimental conditions as shown in Figure 3. For the national filter paper with a pore size of 20 µm, a larger aluminum frame (60 cm × 40 cm) was employed. Each frame was mounted on 2 triangular wooden supports equipped with adjustable screws, allowing the frames to rotate freely. Once the desired inclination angle was selected, the frame was fixed in position using the same screws. Also, to evaluate the influence of gravity on the imbibition process, the porous medium was inclined at an angle of 80° with respect to the horizontal. This configuration enables the analysis of the dynamic evolution of the fluid flow over the porous plane while explicitly accounting for gravitational effects.

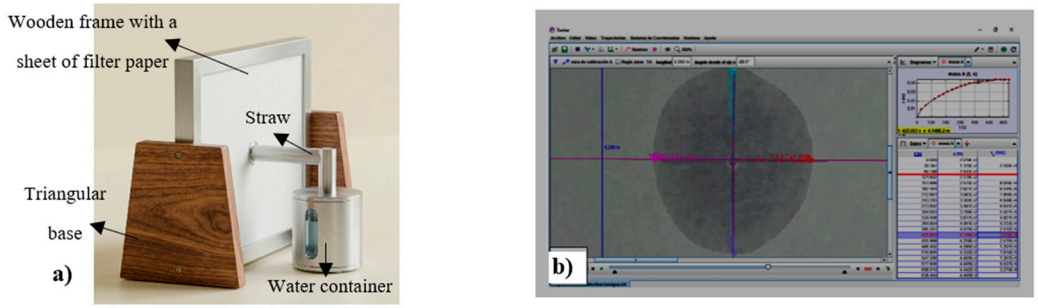


Figure 3. (**a**) Diagram of the experimental setup, and (**b**) visualization of the Tracker program, sample for each Cartesian axis.

The experimental data were used to develop an empirical model based on position–time relationships, which was then compared with the theoretical predictions given by Equation (2). Filter paper was chosen as the porous medium due to its fibrous composition of randomly oriented fibers, enabling effective modeling as an assembly of capillaries and the application of Washburn's theory.

The pore size and thickness of each filter paper were as follows: Whatman filter paper, 2.5 µm pore size and thickness D = 1.92 × 10^{-2} cm; Whatman filter paper, 11 µm pore size and thickness, D = 1.76 × 10^{-2} cm; and national filter paper with 20 µm pore size and thickness, D = 4.35 × 10^{-2} cm (Figure 3). These thickness values allow the sheets to be considered sufficiently thin such that the imbibition process to be regarded as two-dimensional planar flow. All experiments were performed using purified water as the working fluid, with density of ρ = 0.997 g/cm^3, surface tension of γ = 72.0 dyn/cm, and dynamic viscosity of µ = 8.9 × 10^{-3} g/cm×s.

2.2. Data Collection

After the onset of imbibition, a 10 min video was recorded at 30 f/s (±0.03 s) to capture the initial advance of the wetting front. Subsequently, high-resolution photographs (50 MP) were acquired at 1 min intervals over the next 50 min. To quantify the advance of the imbibition front in the videos and photographs, a video analysis was performed using Tracker image processing software V.2.1 (Open Source Physics) (Figure 3b). This allowed for precise tracking of the wet–dry front on the flat surface along four radial directions.

To obtain the shapes formed on the inclined plane, the procedure involved positioning points along the principal axes (X+, X−, Y+, Y−) on the wetted front. Using the software's geometry fitting tool, a least-squares circular fit was performed to determine the average

radius R of the watermark. The software provides the coordinates of the marked points and the center of the resulting circle. Using this data, the distance from the imbibition point (0.0) to the y-coordinate where the center of the resulting circle lies was calculated.

After the onset of imbibition, a 10 min video was recorded at 30 frames per second to capture the initial advance of the wetting front. Subsequently, high-resolution photographs (50 MP) were acquired at 1 min intervals over the next 50 min. Both video and photographic data were analyzed using Tracker software V.2.1, which enabled precise tracking of the wet–dry front on the planar surface along four radial directions.

From this analysis, as shown in Figure 4, position–time datasets were generated to construct plots depicting the temporal evolution of the imbibition front. As illustrated in Figure 3b, the data processing workflow included superimposing a Cartesian coordinate system (purple) on the filter paper surface, centered at the imbibition point, and using a calibration rod (blue line) to convert pixel measurements to physical units. The wet–dry front was manually tracked along the x- and y-axes in each frame, with the software automatically generating corresponding data tables and position–time plots. All experiments were performed under identical conditions, differing only in the porous medium (i.e., filter paper pore size), and each condition was repeated three times to ensure reproducibility.

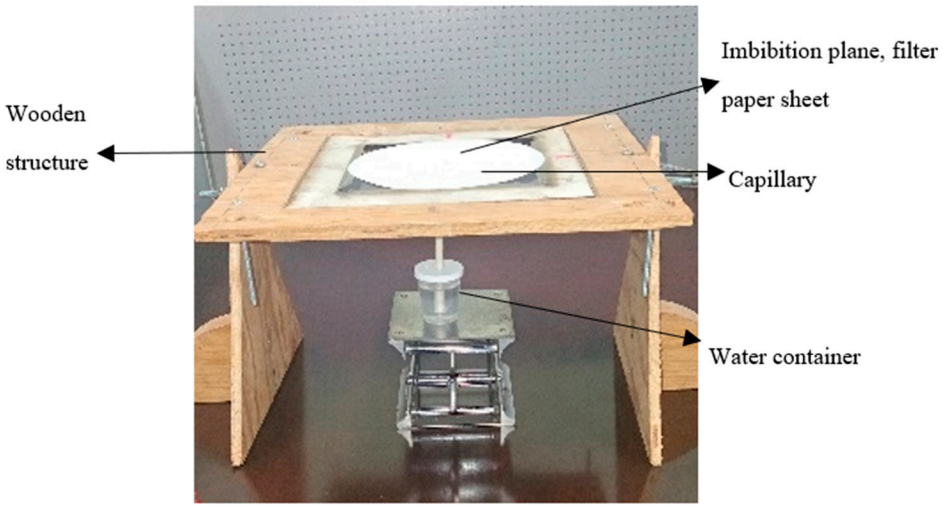


Figure 4. Experimental device when the filter paper sheet is horizontal.

2.3. Concepts and Models

Beyond the classical Washburn model, numerous alternative formulations have been developed to describe capillary imbibition in porous media, each incorporating additional physical parameters. Handy (1960) [18] presented a model that, like Washburn's, predicts fluid advancement proportional to the square root of time, but explicitly includes effects of cross-sectional area, capillary pressure, effective permeability (as defined by Darcy's law), fluid saturation, and dynamic viscosity. Lundblad and Bergman (1997) [19] proposed a model in which imbibition dynamics also follow a square-root-of-time scaling, with explicit consideration of effective pore radius, surface tension, contact angle, and viscosity.

Benavente et al. (2002) [20] formulated a model relating the rate of change in imbibed liquid mass to the cross-sectional area, yielding a square-root dependence on time. This model accounts for porosity, liquid density, statistical effective pore radius, pore shape factor, surface tension, contact angle, viscosity, and tortuosity. In a related study, Li and Horne (2004) [21] demonstrated that the imbibed volume in porous media also scales with the square root of time, considering cross-sectional area, capillary pressure, effective permeability (Darcy), the difference between post-front and initial water saturation, and fluid viscosity. Similarly, Huber (2007) [22] reported square-root-of-time scaling for imbibed

mass, with dependencies on fluid density, surface tension, contact angle, and viscosity. Notably, all these models neglect gravitational effects.

In analyzing these results, the permeability of the porous medium, K, emerges as the primary variable. For filter paper, the pore size refers to the pore diameter (d). Although the exact permeability depends on the manufacturer, a common physical approximation for porous fiber media (such as paper) is to use a relationship proportional to the square of the pore diameter. Furthermore, following the approach of Medina et al. [17]. The volumetric flow rate is defined as the volume of fluid traversing a given surface per unit time, δt is a critical parameter for characterizing the imbibition front. The volumetric flow rate over the surface is provided in Equation (3):

$$\phi = \int_S v \, dA, \tag{3}$$

where v is the local fluid velocity and dA is the differential area element.

In these experiments, the volumetric flow rate represents the radial supply of fluid sustained throughout the imbibition process. By assuming this flow rate is constant, the normalized flow rate can be expressed as shown in Equation (4):

$$\frac{\phi}{D} = 2\pi r v_r, \tag{4}$$

where v_r is the instantaneous radial velocity evaluated at the initial radius, r. In the experiments, this radius was kept constant using a capillary source.

2.4. Physical Problem

At this stage, the evolution of the imbibition front is evaluated as a function of pore size (permeability) and gravity. Permeability K is an intrinsic property of a porous medium related to the ability of a fluid to flow through the material's pores. Generally, permeability is a second-order tensor. In an isotropic medium, permeability is a scalar. Although the medium exhibits microscopic anisotropy, for the purposes of this study, effective isotropy was assumed. This is because the characteristic length of the experiment ($L \approx 10$ cm) is several orders of magnitude greater than the Representative Element Size (RES) of the pore, allowing for a homogeneous continuous medium approximation.

To rigorously characterize the imbibition front dynamics, it is necessary to employ the governing equations for flow in porous media, beginning with the momentum conservation equation, commonly referred to as Darcy's law (Equation (5)) [23].

$$v = \frac{K}{\mu} \nabla P, \tag{5}$$

Here μ is the dynamic viscosity of the fluid. Equation (6) establishes that fluid velocity is proportional to pressure gradient, with a proportionality factor determined by the medium's permeability and the fluid viscosity. To account for gravitational effects, Darcy's law is extended by incorporating a gravitational term, as reflected in Equation (6).

$$v = \frac{K}{\mu} \nabla P + \nabla \rho g, \tag{6}$$

where ρ is the fluid density, and g is gravitational acceleration.

In addition to Darcy's law, theoretical analysis of the problem requires a second fundamental equation: mass conservation. For an incompressible fluid with constant

density, the time derivative of density is zero, simplifying the continuity equation to the form presented in Equation (7).

$$\nabla v = 0, \tag{7}$$

Combining Equations (5) and (7) yields Laplace's equation for the pressure field, $\nabla^2 P = 0$. Solving this equation analytically is highly complex due to the nonlinearities imposed by the geometry and boundary conditions of the imbibition problem. Richards (1931) [24] first combined Darcy's law with the continuity equation for unsaturated flow, resulting in a nonlinear diffusion equation that states that the advance of the fluid is governed solely by the equilibrium between the gravitational and capillary potentials. As a result, many studies have relied on numerical methods and computational simulations to address these challenges. In this work, emphasis is placed on experimental results, which are then compared with the theoretical solution proposed by Medina [17].

3. Experimental Results

Each experiment was conducted in triplicate under controlled laboratory conditions. A total of 18 experiments were conducted at room temperature, with relative humidity maintained at (45 ± 5)% and ambient temperature at 25 ± 3 °C, representing average values for the duration of the study. The results are organized in two primary stages. First, data from horizontal filter paper sheets were analyzed to determine the temporal exponent governing the advance of the imbibition front for each pore size. Second, the experiments with the filter paper inclined at 80° relative to the horizontal were conducted to quantify the influence of gravity on imbibition. Also, imbibition front profiles were measured along four directions aligned with the axes of a Cartesian coordinate system, with the origin at the imbibition point and the y-axis oriented downward. For the inclined configuration, particular emphasis was placed on the evolution of the imbibition front along the y-axis to isolate and quantify gravitational effects.

3.1. Porous Medium Without Inclination

Figure 5 illustrates the evolution of the wet–dry imbibition front r_s along each Cartesian axis. Without inclination, the imbibition process demonstrates radial symmetry, with similar advancement observed in all directions. Accordingly, front positions from each axis were averaged to provide a representative radial progression.

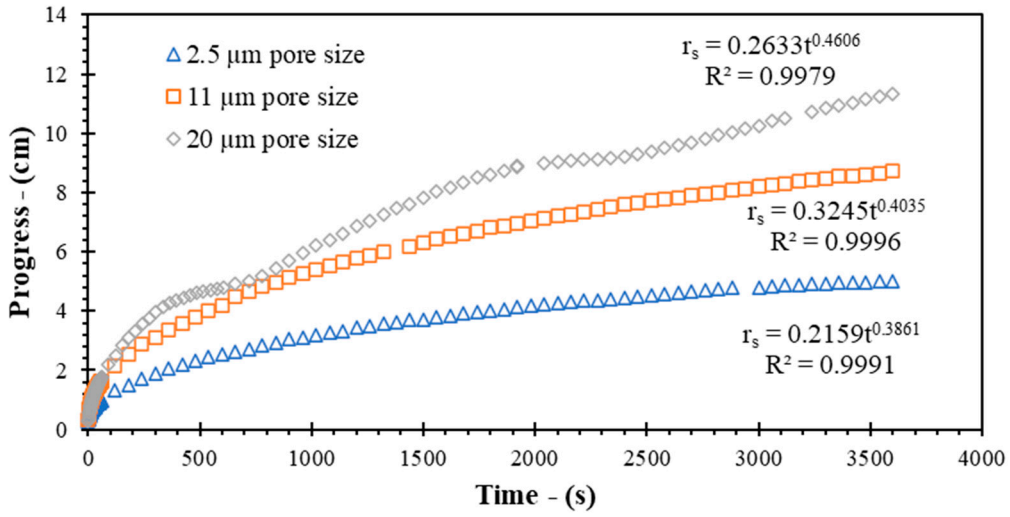


Figure 5. Average progression of the wet–dry front as a function of time for various pore sizes over 60 min.

For each pore size, distinct empirical relationships were established, reflecting the different permeabilities of the filter papers. These empirical models characterize imbibition dynamics in the absence of gravitational influence. Notably, for the filter paper with a pore size of 20 µm, the temporal evolution of the imbibition front, $r_s = 0.2633\ t^n$, $n = 0.4606 \pm 0.000084$ (95% CI), yields an exponent closest to the theoretical value of 1/2 predicted by the Washburn model. The exponents' uncertainties reflect 95% confidence intervals. They are based on propagated instrumental errors, which are negligible due to the camera's 30 fps resolution and the Tracker software's sub-pixel accuracy.

Additionally, a series of time-lapse photography clearly demonstrates the radial progression of the imbibition process (Figure 6). Tracker software was employed to quantify the geometric characteristics of the imbibition mark, confirming a circular front whose center coincides with the imbibition point. The imbibition mark consistently exhibits a circular geometry, demonstrating that fluid advancement proceeds as uniform horizontal propagation in all directions from the imbibition point.

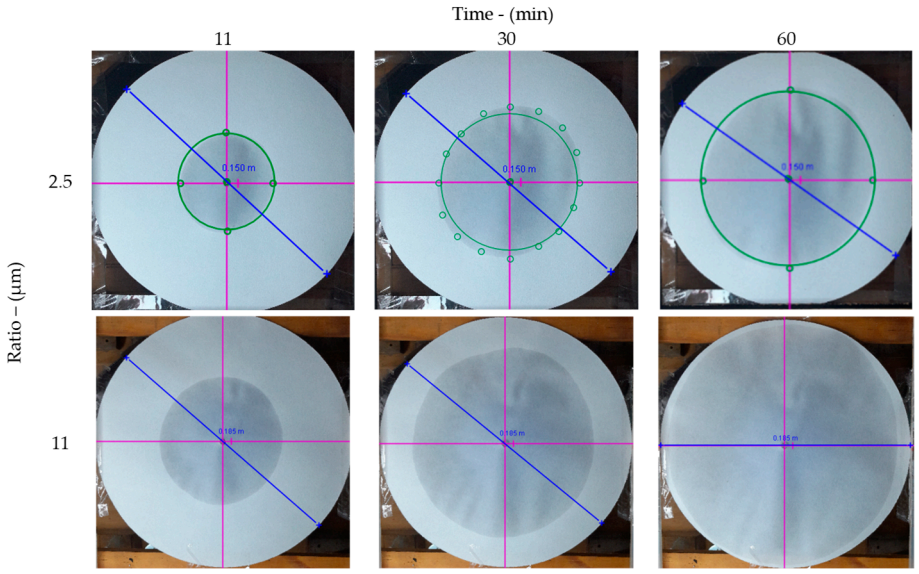


Figure 6. Whatman filter paper imbibition process.

Figure 7 displays a time series of photographs capturing the imbibition pattern on national filter paper with a 20 µm pore size under non-inclined conditions. The imbibition mark consistently exhibits a circular geometry, demonstrating that fluid advancement proceeds as uniform horizontal propagation in all directions from the imbibition point.

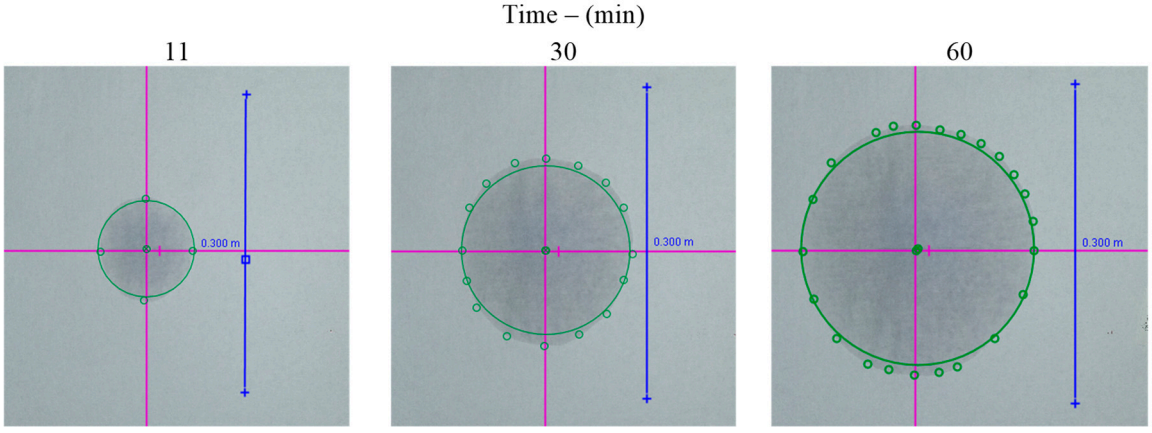


Figure 7. Imbibition marks on 20 µm national filter paper.

3.2. Porous Medium Inclined at 80°

Figure 8 presents the results for the Whatman filter paper with a pore size of 2.5 µm over a 40 min experimental period. The curves depict the progression of the wet–dry imbibition front along each direction as a function of time. Notably, the greatest advancement occurs along the negative y-direction (y^-), reaching approximately ~4 cm, while the positive-direction y-direction (y^+) attains about 2.5 cm. The remaining directions, x^+ and x^-, show intermediate advances of roughly 2.86 cm and 3.07 cm, respectively.

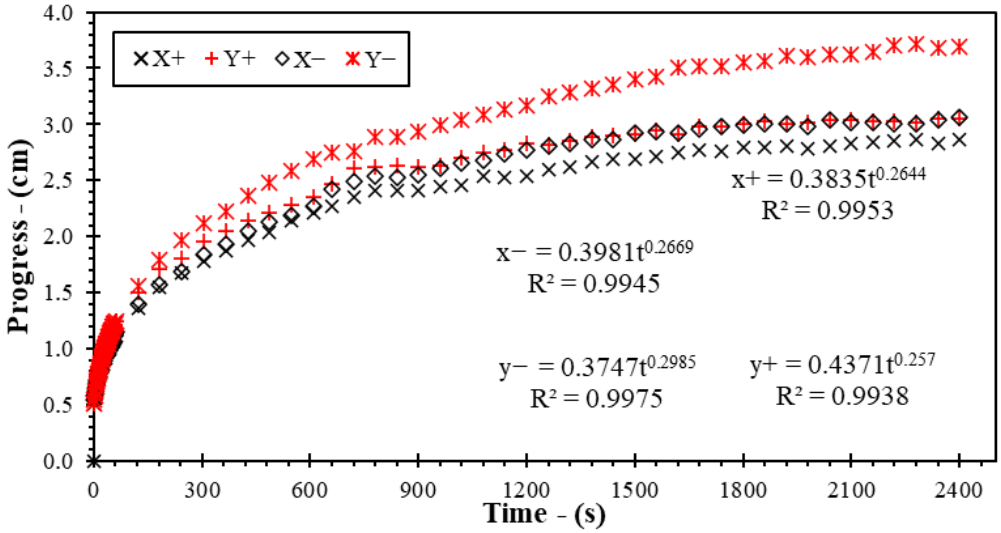


Figure 8. Progression of the wet–dry front on 2.5 µm Whatman filter paper at an 80° inclination over 40 min.

The pronounced advancement along the y^--direction is attributed to the combined effects of the pressure gradient and gravity, as described by Equation (6). When the plane is inclined, gravity acts as an additional driving force downslope, resulting in a higher effective pressure gradient and, consequently, a greater imbibition distance in this direction than in others. Despite these directional differences, the imbibition front in all directions exhibits a power law dependence on time, with a temporal exponent of approximately 0.26, indicating a substantial deviation from classical Washburn scaling under inclined conditions.

At various time intervals, photographs of the water imprint were obtained, and the front positions measured along each axis were used to fit a circle. In contrast to the non-inclined scenario, where the center of the circular pattern aligns with the imbibition point, the inclined configuration reveals a downward shift in the circle's center relative to the imbibition point (Figure 9). The measured displacement of the center, 0.419 cm, quantifies the effect of gravity on the imbibition of front geometry.

Figure 10 shows the evolution of the imbibition front in Whatman filter paper with a pore size of 11 µm over a 45 min experimental period. The progression of the wet–dry front is depicted along four directions originating from the imbibition point. Notably, the greatest advancement is observed along the negative direction (y^-), which aligns with gravity, reaching approximately 5.63 cm, while the other directions exhibit advances of about 5 cm. These findings demonstrate that gravity significantly enhances fluid penetration downslope. Circular fitting of the water imprint on the 11 µm Whatman filter paper reveals a downward displacement of the circle's center by 0.500 cm relative to the imbibition point, quantifying the effect of gravity on the imbibition front geometry.

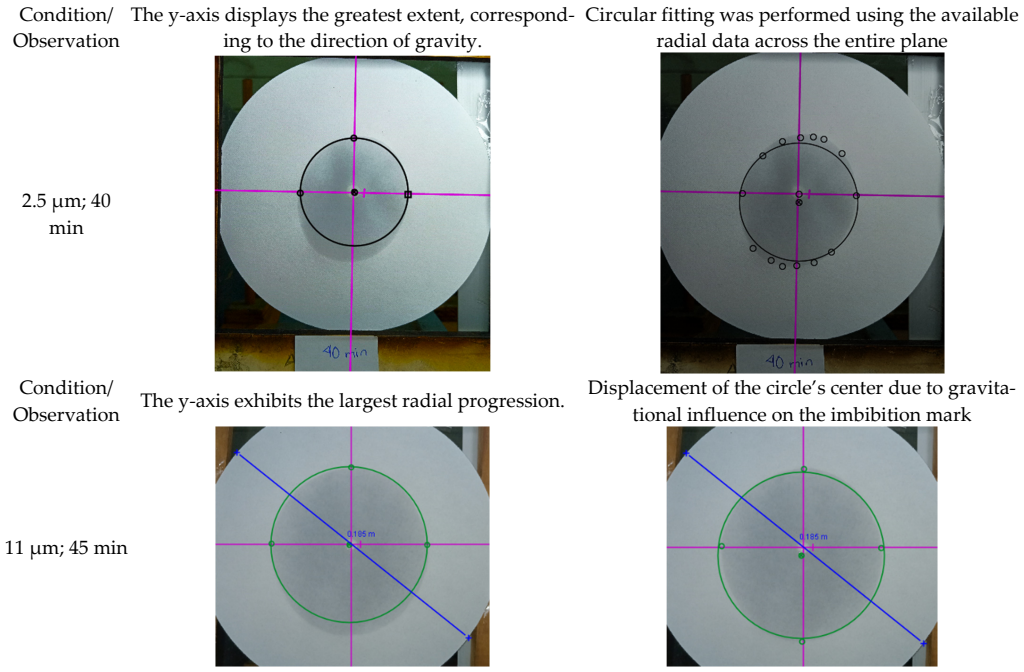


Figure 9. Imbibition patterns for Whatman filter paper with pore sizes of 2.5 µm and 11 µm under experimental conditions.

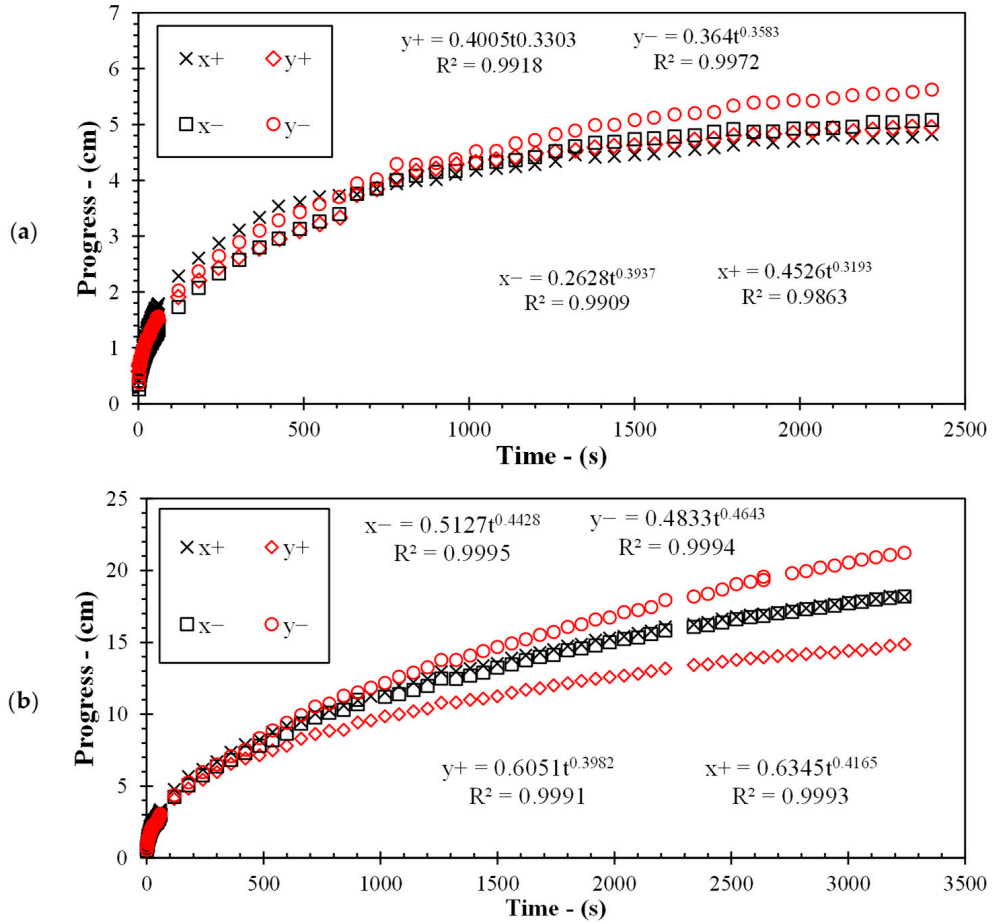


Figure 10. Temporal evolution of the wet–dry front: (**a**) Whatman filter paper (11 µm pore size) inclined at 80° to the horizontal, tracked over 40 min and (**b**) wet–dry front progression during imbibition in national filter paper (20 µm pore size) over 54 min. The difference in the total duration of the experiments is dictated by the physical dimensions of the substrates used.

Figure 9 presents the evolution of the imbibition front for the national filter paper with a pore size of 20 μm, highlighting the pronounced influence of gravity in this configuration. Along with the positive y direction (y^+ opposite to gravity), the front advances to approximately 14.9 cm, which is less than the advances observed in other directions and is associated with a lower time exponent. In contrast, along the negative y direction (aligne), the imbibition front reaches a maximum distance of approximately 21.2 cm and displays the largest temporal exponent. These results clearly demonstrate the strong coupling between gravity and permeability in highly permeable porous media.

Figure 11 demonstrates that, after 54 min, the imbibition mark maintains an approximately circular shape, but its center is displaced downward relative to the imbibition point. Throughout the experiment, the imbibition patterns consistently remain circular; however, the inclination of the paper sheet causes gravity to induce a downward translation of the circle's center. The measured displacement of 3.545 cm underscores the pronounced impact of gravity in highly permeable porous media.

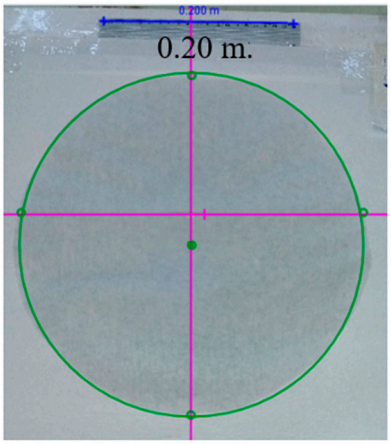


Figure 11. Imbibition mark observed after 54 min on a 20 μm pore size filter paper sheet.

4. Analysis and Discussions

4.1. Case 1. Plane Without Inclination

For all three types of filter paper analyzed (2.5 μm, 11 μm, and 20 μm) under non-inclined conditions, as summarized in Table 1, the advance of the imbibition front was nearly identical in all directions at any given time. Throughout all experimental repetitions, a consistent radial propagation pattern was observed, indicating homogeneous fluid distribution across the horizontal plane.

Table 1. Temporal exponent values for each filter paper with varying permeability. The permeability (K) was estimated based on the nominal pore radius (r) using the relation $K = \frac{\Phi \cdot r^2}{8}$, where φ is the porosity of the material [5].

Exponent of Time	Pore Size—(μm)	Permeability K—(cm^2) [ϕ = 0.7]	Observations
0.3861	2.5	1.37×10^{-09}	This sample displays the slowest imbibition front progression and the greatest deviation from the Washburn law.
0.4035	11	2.65×10^{-08}	Displays intermediate imbibition advancement; the temporal exponent increases with increasing pore size.
0.4606	20	8.75×10^{-08}	Exhibits the greatest imbibition front progression and a temporal exponent closest to the theoretical value of 0.5 ($t^{0.5}$).

The analysis of the imbibition length as a function of time revealed a power law relationship, with temporal exponents consistently below the theoretical value of 1/2 predicted by the Lucas–Washburn equation (Equation (1)). This deviation is primarily attributed to the permeability and pore size of the medium, which are the dominant factors governing imbibition dynamics. In particular, smaller pore sizes (2.5 μm) result in substantially slower fluid front advancement, while larger pores (20 μm) yield a higher imbibition rate and temporal exponents approaching 0.5, with typical values around ~0.4.

Numerical results reported by Fries and Dreyer (2008) [5], although obtained with fluids other than water, also yield temporal exponents lower than those predicted by the Lucas–Washburn model, corroborating the trends identified in this study. Because these values represent averages over the four principal directions, the imbibition process can be effectively modeled as horizontal advancement in the absence of gravitational effects. Table 1 summarizes the average temporal exponents, along with the corresponding pore sizes and permeabilities. The data reveal a clear trend: as pore size and permeability increase, the temporal exponent rises, approaching the theoretical value of 1/2.

Previous studies, such as those by Cai and Yu (2011) [6], have linked the temporal exponent to parameters such as tortuosity and the fractal dimension of the porous medium. In contrast, the present work focuses on the role of effective permeability, which yields similar exponent values. For example, Balankin et al. (2006) [25] reported temporal exponents of 0.41 and 0.38 for filter paper, values that closely align with those obtained in this study for pore sizes of 11 μm (0.4035) and 2.5 μm (0.3861), with relative deviations of only 2.35% and 2.39%. Furthermore, HoryPath and Stanley [26] reported a temporal exponent of 0.386 for filter paper, which closely matches the value found here for the 2.5 μm pore size, suggesting that their results likely pertain to a similar filter medium.

The ideal Washburn theory predicts that imbibition length scales with the square root of time ($t^{0.5}$). However, both the literature reports and the experimental results presented here show that, in real porous media, the temporal exponent is typically less than 0.5 and is strongly influenced by the permeability and structural characteristics of the medium. The present findings confirm that increasing pore size and permeability result in larger temporal exponents that approach the theoretical Washburn value. Furthermore, under inclined configurations, the imbibition pattern deviates from a concentric circular geometry, with the imbibition front center shifting toward the gravity vector. This displacement becomes substantially more pronounced in media with larger pores and higher permeability, as evidenced by an increase in displacement from the imbibition point of 0.497 cm to 3.545 cm when the pore size increases from 11 μm to 20 μm. Regarding imbibition velocity, the results demonstrate that smaller pores (2.5 μm) lead to a markedly slower advance of the fluid front, while larger pores (20 μm) facilitate faster dynamics that more closely align with Washburn's theoretical prediction.

Table 2 summarizes temporal exponent values for capillary imbibition in paper-based porous media as reported in the literature. Balankin et al. [25] observed exponents ranging from 0.38 to 0.41, corresponding to different imbibition regimes including precursor film flow and bulk front propagation. Horváth and Stanley [26] reported a temporal exponent of 0.386 for filter paper, and Lam and Horváth [27] found a similar value of 0.382 for paper substrates. All these exponents are lower than the theoretical value of 0.5 predicted by the Lucas–Washburn model, reinforcing that capillary imbibition in real porous media is characterized by sub-diffusive behavior, predominantly influenced by the medium's structural features.

Table 2. Reported temporal exponent values from various capillary imbibition studies in paper-based porous media.

Time Exponent	Porous Media	Author	Source
0.41 *–0.38 **	Paper	Balankin et al. (2006)	[25]
0.386	Filter paper	Horváth and Stanley (1995)	[26]
0.382	Paper	Lam and Horváth (2000)	[27]

Note: * Transient precursor film flow, and ** Transient bulk impregnation main front and saturation stage.

The theoretical model developed by Medina [17] predicts a critical time interval during which the formulation remains applicable, even in the presence of gravitational effects. In this study, the critical time is both calculated and directly compared with experimental observations. The critical time is defined as Equation (8):

$$t_c = \frac{\phi(4\pi D)}{\left(\frac{\rho g \cos(\alpha)\cos(\theta)K}{\mu}\right)^2}, \quad (8)$$

where ϕ denotes the volumetric flow rate, D is the porous medium thickness, ρ is the fluid density, α is the inclination angle relative to the horizontal, and θ represents the angular position in the plane (polar coordinates).

Figure 11 compares experimental models with theoretical predictions. As discussed earlier, the experiments exhibit distinct behaviors for each porous medium as a function of pore size. Notably, during the initial stages of imbibition, the theoretical model accurately captures the experimental data. The calculated critical time is $t_c \approx 9$ s, and, as illustrated in Figure 12, all experimental curves coincide with the theoretical model over this time interval.

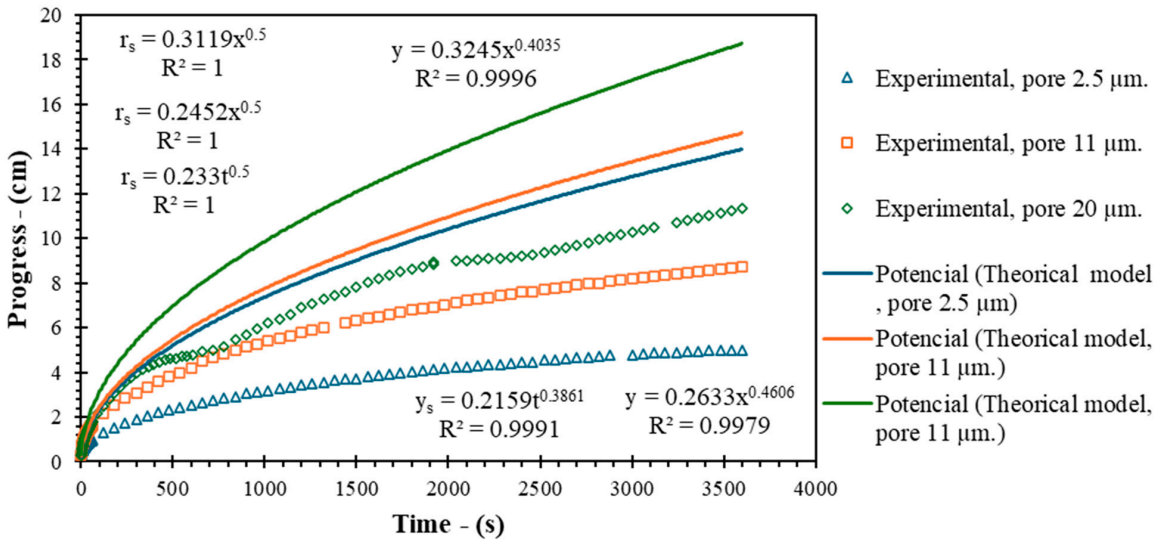


Figure 12. Comparison of experimental and theoretical models for all pore sizes under non-inclined conditions over a 60 min period.

Accordingly, plotting the first 9 s of experimental data against the theoretical model reveals partial agreement at early times (see Figure 12). Detailed analysis of imbibition behavior shows that, in the experiments, the volumetric flow rate decreases over time, whereas the theoretical model assumes a constant flow rate. This difference is a primary factor underlying the divergence between experimental and theoretical predictions at longer times. The greater advance observed in our experiments during the first 9 s is attributed to the "inlet effect" or "initial surge" that analytical models typically overlook. In the first

few seconds, the fluid expands almost instantaneously. This is the initial impulse that A. Medina's model (which is macroscopic) fails to capture. At $t \to 0$, the contact between the water and the porous matrix generates high initial capillary suction and a slight local hydrostatic pressure due to the fluid volume, resulting in an initial volumetric flow rate that exceeds the theoretical prediction. As the front advances and viscous resistance increases, the flow rate stabilizes and eventually decreases.

Another critical variable is pore size, which was systematically varied in this study. Experimentally, the imbibition front progression deviated from a strict square-root-of-time dependence, instead exhibiting a lower temporal exponent that varied with the porous medium. In contrast, the theoretical model maintains a fixed temporal exponent, with only the time coefficient varying. These findings account for the observed differences between the experimental and theoretical curves in Figure 13 and indicate that permeability should be incorporated into the temporal exponent, while the volumetric flow rate should be incorporated into the time coefficient.

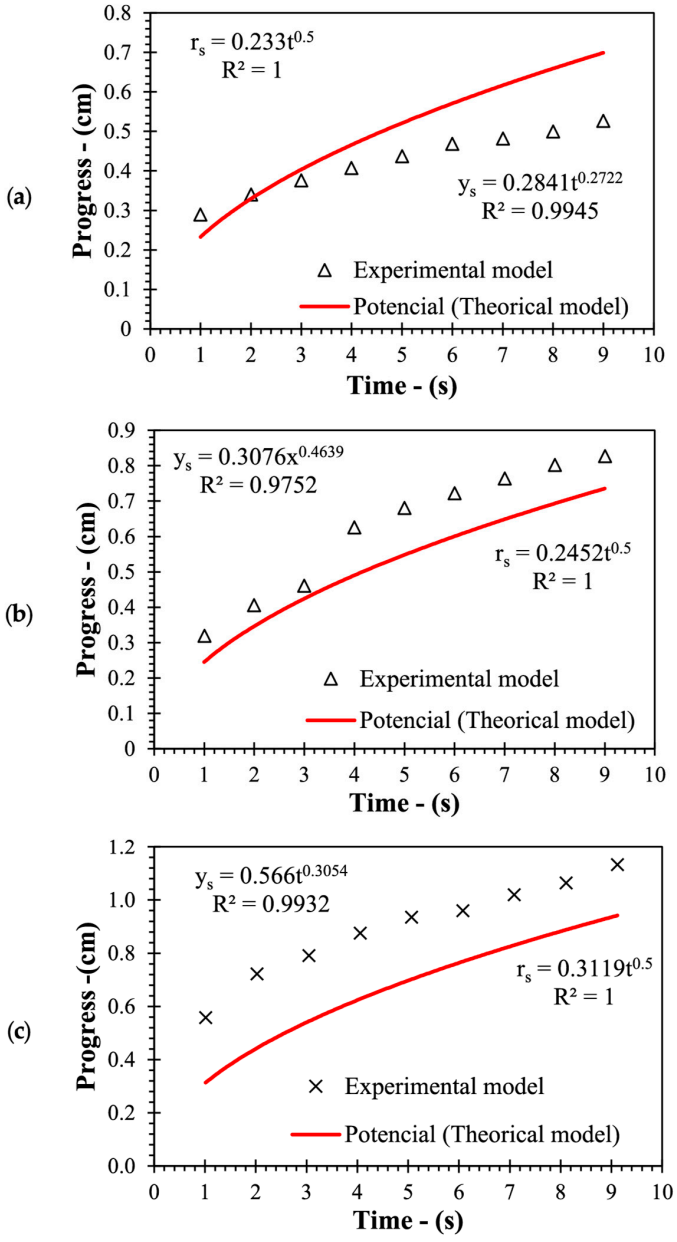


Figure 13. Comparison of theoretical and experimental imbibition models during the first 9 s, (**a**) Whatman 2.5 μm filter paper, (**b**) Whatman 11 μm filter paper, and (**c**) National 20 μm filter paper.

As outlined in the introduction, numerous theoretical models have been proposed, each incorporating different physical parameters and yielding distinct formulations. Despite these differences, a common assumption is that fluid advancement scales with the square root of time [13–17]. However, the present study demonstrates that the imbibition front exhibits a more general power law behavior, with a temporal exponent that depends explicitly on both pore size and gravity.

Specifically, the evolution of the imbibition front can be described by a relation of the form $f(t) = At^b$ with $0 < b < 1/2$, where A and b are empirically determined parameters associated with the pore size of the porous medium. The use of water as the working fluid ensures constant surface tension, density, and viscosity across all experiments, resulting in highly consistent and reproducible imbibition dynamics for filter papers with the three different permeabilities studied.

The study by Benavente (2002) [20] also relies on measurements of porous structure; however, a direct comparison is not feasible since their model predicts the absorbed water per unit area and reports mass uptake rates, whereas the current work focuses on the temporal evolution of the imbibition front as a function of pore size. Similarly, Huber (2007) [22] investigated capillary rise in linear alkanes within nanoporous monolithic Vycor glass (mean pore radius of 5 nm). The measurements of mass uptake as a function of time, $m(t)$, were consistent with the classical Lucas–Washburn $\sqrt{t}$ scaling typical of liquid imbibition in porous media. In contrast, the present results show that, under specific conditions involving gravity and permeability, the progression of the imbibition front deviates from a strict square-root-of-time dependence.

4.2. Inclined Plane at 80°

As in the non-inclined configuration, a time exponent analysis was conducted for the inclined case. The results reveal that the temporal exponent increases with pore size, reflecting more vigorous imbibition dynamics in highly permeable media. Moreover, for any given porous medium, the exponent is consistently higher along the downslope direction (y^-), where gravity enhances fluid flow.

As summarized in Table 3, the temporal exponent increases with both permeability and alignment with the direction of gravity. These findings align with results reported by Horne and Stanford (2001) [21], who demonstrated that gravitational effects are significant in imbibition processes, based on experiments with packed glass microspheres that showed a deviation of the imbibition front origin from zero. A similar trend is observed in the current study, where gravity acts preferentially along the y^--axis when the filter paper is inclined at 80° to the horizontal. Horne and Stanford concluded that water imbibition is governed by capillary pressure and relative permeability, which are associated with different saturation states within the porous medium. The present results further demonstrate that spontaneous imbibition is governed by capillary pressure and the medium's intrinsic permeability, with gravity playing a crucial role in modulating imbibition dynamics under inclined conditions. Statistical comparison using Student's *t*-test confirmed that the observed trends are significant, ruling out instrumental uncertainty as the cause of the variations in the power law. The fact that the difference is greater in 20 μm pores validates the hypothesis that permeability and gravitational force compete more effectively against capillary pressure at larger radii.

Furthermore, the comparison between experimental and theoretical models was extended to the inclined plane, employing the same methodology as for the non-inclined configuration. A key implication of the theoretical model is that, under the assumption of a constant volumetric flow rate, the imbibition process is predicted to advance uniformly in all directions, irrespective of gravitational effects.

Table 3. Temporal exponents for each Cartesian direction in various porous media at an 80° inclination angle.

Slope	Pore Size—(μm)	Cartesian Coordinate Axis	Exponent
80°	2.5	$x+$	0.264
		$y+$	0.257
		$x-$	0.267
		$y-$	0.299
	11	$x+$	0.319
		$y+$	0.330
		$x-$	0.394
		$y-$	0.358
	20	$x+$	0.417
		$y+$	0.398
		$x-$	0.443
		$y-$	0.464

Figure 14 illustrates the experimental progression of the wet–dry front during the initial seconds of imbibition, as captured by measured data points along four planar directions. The results show that the front advances nearly identically in all directions, with differences limited to one or two millimeters. This finding indicates that, in the early stages of imbibition, the inclination of the plane exerts a negligible influence, and the front's advance can be considered directionally uniform.

Comparison with theoretical predictions reveals discrepancies for both the Whatman filter paper (2.5 μm pore size) and the national filter paper (20 μm pore size). In contrast, the 11 μm filter paper exhibits close agreement between the theoretical model and experimental results during the initial time interval. These observations underscore the sensitivity of the theoretical model to permeability variations and its underlying assumptions, particularly the presumption of a constant volumetric flow rate of 4.3 for volumetric flow rate analysis for the non-inclined filter paper.

4.3. Volumetric Flow Rate Analysis for the Non-Inclined Filter Paper

The volumetric flow rate was determined by analyzing changes in the imbibition front position along each Cartesian axis. Because imbibition under non-inclined conditions is radially symmetric, the radius along each axis was considered only during the first second of the process, when it closely matches the initial radius. Although the front advances according to a power law relationship, the volumetric flow rate decreases markedly at longer times because it depends on the instantaneous velocity (see Equation (4)). Experimental models consistently show a decline in velocity over time, confirming that the volumetric flow rate is not constant. Thus, the flow rate was evaluated exclusively at early times (t = 1 s). Li, Horne, and Stanford (2001) [21] reported similar findings in water imbibition experiments with Berea sandstone and glass bead packs: they observed a maximum water uptake rate initially, followed by a gradual decline to near constancy. This behavior further supports the conclusion that the volumetric flow rate decreases as imbibition progresses.

Equation (4) was employed to calculate the volumetric flow rate, assuming radial symmetry and constant velocity at the initial time. Figure 15 displays a bar chart, with each bar representing a Cartesian axis. The volumetric flow rates are nearly identical across all directions; however, the value along the x-axis is marginally higher, differing by approx-

imately one part in a thousand. This slight discrepancy may result from the preferential alignment of capillaries generated during the paper manufacturing process. Similarly, for the 11 µm filter paper, Figure 15 shows that volumetric flow rates are nearly uniform across all axes, with only one direction showing a comparatively small deviation. As before, this minor difference is likely attributable to anisotropies introduced during fabrication.

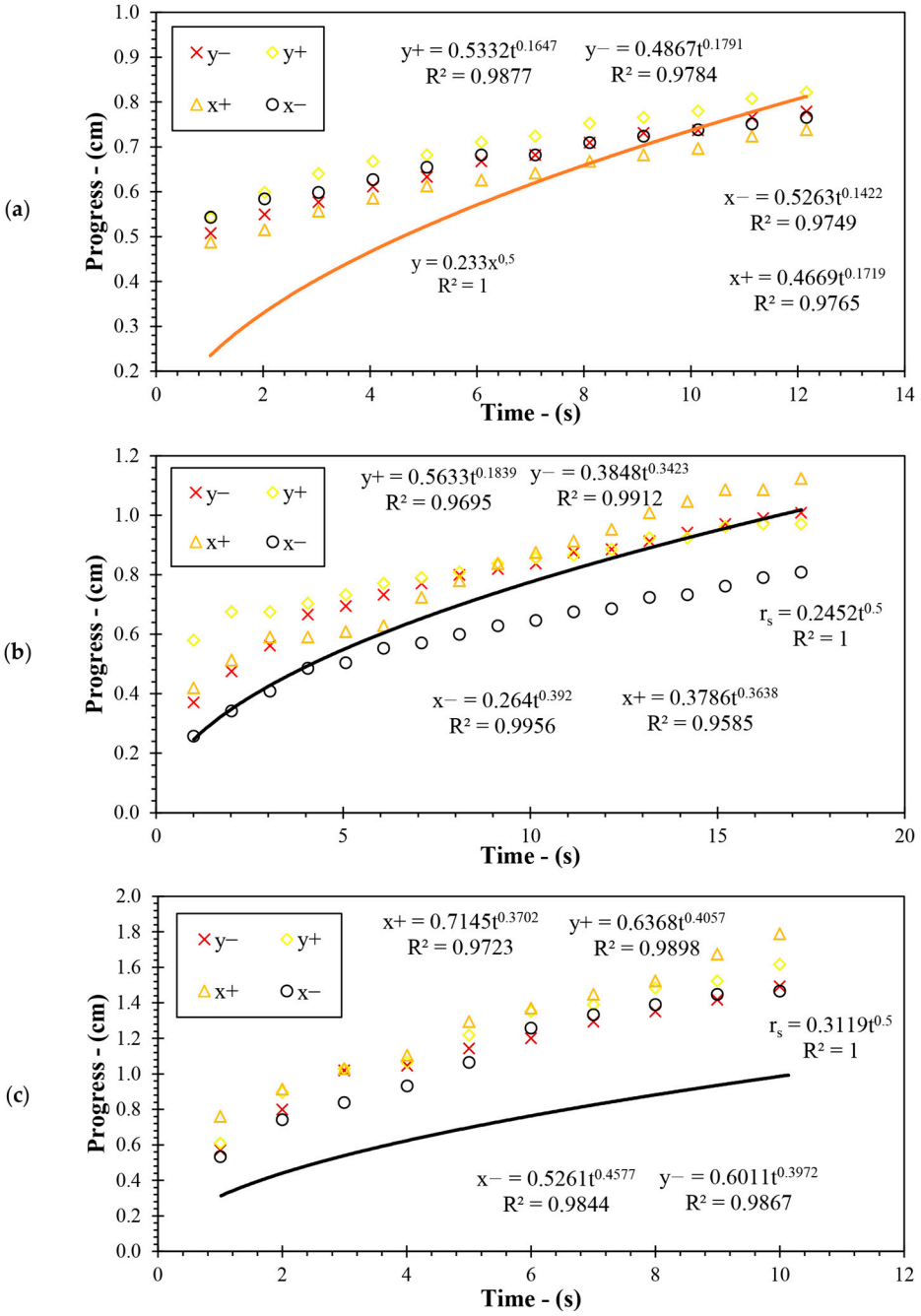


Figure 14. Experimental progression of wet–dry front in all four directions compared to the theoretical model for imbibition at an 80° inclination: (**a**) 2.5 µm Whatman filter paper, (**b**) 11 µm Whatman filter paper, and (**c**) 20 µm National filter paper.

4.4. Volumetric Flow Rate Analysis for the Filter Paper at an 80° Inclination

Each experiment was conducted in triplicate under identical conditions to ensure reproducibility and consistency of the results. High repeatability was observed across all cases, indicating that the imbibition process maintains radial symmetry during the early stages, even when the paper sheet is inclined at 80°. Therefore, at initial times,

it is reasonable to assume the same radius along all four directions, enabling accurate calculation of the volumetric flow rate.

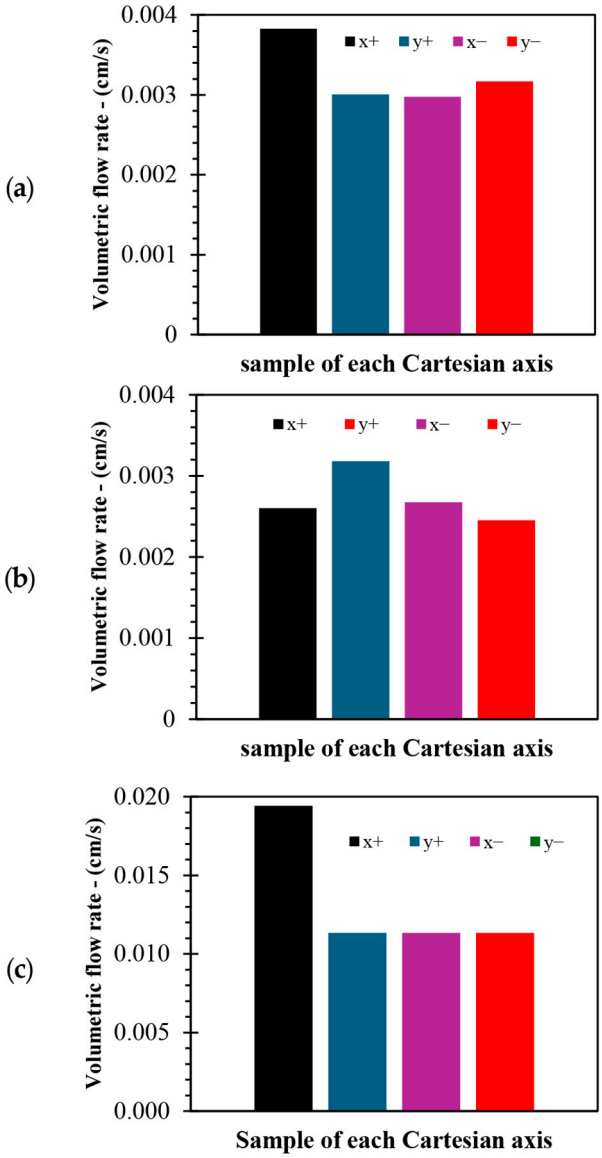


Figure 15. Volumetric for filter paper sheet of: (**a**) 2.5 µm, (**b**) 11 µm, and (**c**) 20 µm.

Figure 16 presents bar charts of the volumetric flow rate for Whatman filter papers with pore sizes of 2.5 µm, 11 µm, and 20 µm. At early times, the flow rate is nearly identical along all axes for the 2.5 µm paper, indicating uniform fluid advancement and negligible gravitational effects at the onset of imbibition. Minor differences, approximately of ± 0.002 cm/s, are attributed to the preferential orientation of fibers introduced during paper manufacturing, consistent with observations in the non-inclined case. For the 11 µm filter paper, differences between axes increase to around ± 0.005 cm/s, while for the 20 µm paper, differences reach about ± 0.020 cm/s. Although these deviations are more pronounced in papers with larger pore sizes, they do not show a systematic dependence on capillary forces or gravity; the axes with the largest differences vary randomly. This pattern further supports the conclusion that the observed variations primarily arise from structural anisotropies inherent to the paper fabrication process (see Figure 16).

While numerous studies in the literature describe imbibition dynamics using the imbibed water mass, direct comparison with the present results is difficult. This is primarily

because those studies were conducted in porous media other than filter paper or did not explicitly consider gravitational effects [20–22].

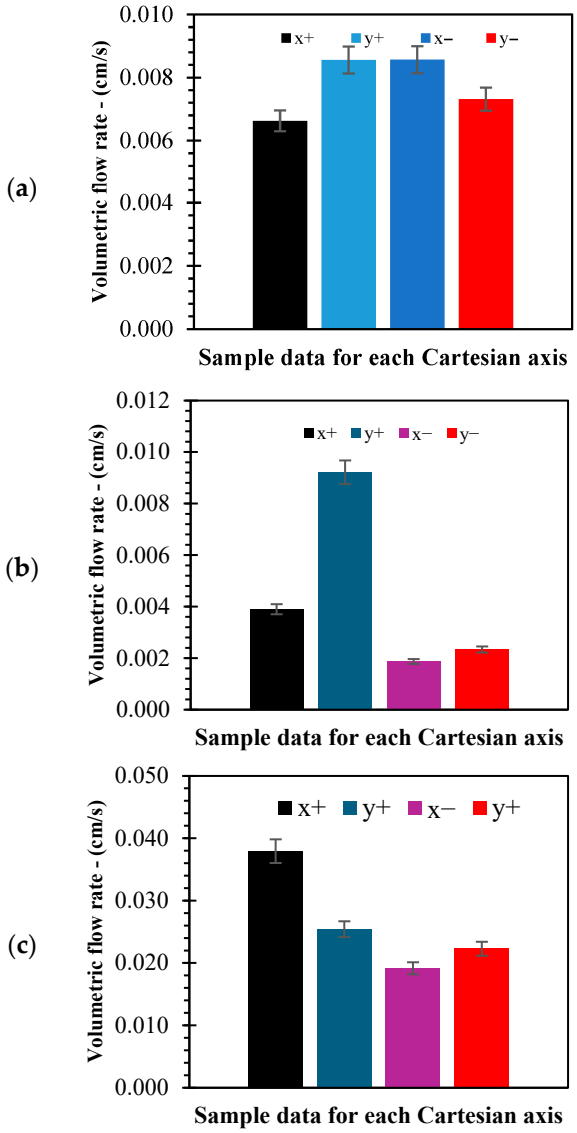


Figure 16. Volumetric flow rate for the filter paper sheet for t = 1 s of: (**a**) 2.5 µm, (**b**) 11 µm, and (**c**) 20 µm.

5. Conclusions

The results demonstrate that imbibition is a complex process governed by multiple interacting variables, making it challenging to establish a single universal curve for spontaneous imbibition. The observed dynamics are highly sensitive to the specific variables incorporated in each model. This study focused on the roles of pore size (permeability) and gravitational effects. For all experimental cases, empirical advancement equations were derived, each characterized by unique time exponents and coefficients. These models consistently exhibited excellent agreement with the experimental data, as indicated by high correlation coefficients.

A comprehensive series of imbibition experiments was conducted to examine the correlation between medium permeability and gravity. For non-inclined porous media, the temporal exponent was determined to be 0.3861 for Whatman filter paper with a 2.5 µm pore size, 0.4035 for 11 µm, and 0.4606 for national filter paper with 20 µm pores. These findings reveal that the temporal exponent increases with pore size, highlighting a direct

dependence of imbibition dynamics on the medium's permeability. Comparisons with previous studies ([25–27]) yielded deviations of 2.39% and 2.35%, attributable to variations in experimental conditions and porous structures. Furthermore, the imbibition patterns consistently exhibited circular geometry, with the center aligned with the imbibition point, thereby confirming radial symmetry in the absence of gravity.

A comparison of the experimental results with the theoretical model proposed by Medina et al. [17] revealed discrepancies at longer times. However, after calculating the critical time, estimated at approximately 8 s, moderate quantitative agreement between experimental and theoretical predictions was observed within this initial interval. The percentage errors between the models were 19.8% for the 2.5 μm filter paper, 16% for the 11 μm paper, and 26.5% for the 20 μm paper. The greater deviation observed for the largest pore size correlates with its greater imbibition advance over the same time period, reflecting the amplified effects of gravity and permeability that are not fully accounted for in the theoretical model.

For the porous medium inclined at 80°, temporal exponents measured in the direction of gravity were higher than those in the non-inclined configuration, demonstrating that gravity markedly enhances imbibition advancement. While the imbibition front maintained a generally circular shape, its center was consistently displaced downward relative to the imbibition point, thereby quantifying the gravitational effect. The measured center displacements were 0.419 cm for 2.5 μm, 0.497 cm for 11 μm, and 3.545 cm for 20 μm pore sizes, revealing that displacement increases with pore size.

The experimental results presented here contribute to our understanding of water flow behavior in porous media on the micrometer scale. The pore size is comparable to that of porous, permeable rocks such as sandstones, limestones, and dolomites (carbonate rocks), in which hydrocarbons accumulate after migration. Rocks like shales and limestones also exhibit fractures on the order of a few tens of micrometers.

In summary, these results establish permeability and gravitational potential as primary determinants of fluid dynamics during imbibition. Although imbibition is inherently complex, this study advances the understanding of the coupled effects of pore size and gravitational potential on the propagation of the wetting front. Future research should investigate the impact of additional variables, such as fluid properties, contact angle, medium anisotropy, and saturation effects, to further refine theoretical models and broaden insight into imbibition phenomena in porous materials.

The experimental datasets presented in this study provide a robust foundation for future integration into machine learning (ML) frameworks. Furthermore, these results offer a simplified benchmark for ML models aimed at addressing complex flow problems in reservoir engineering and enhanced oil recovery (EOR), where accurate physical constraints are essential for predictive reliability.

Future efforts will focus on expanding the dataset to include a wider range of pore sizes and intermediate inclination angles $(0° < \theta < 90°)$. This will enable the development of a generalized semi-empirical model for predicting fluid transport and runoff thresholds in paper-based microfluidic devices under diverse gravitational orientations.

Author Contributions: J.J.M.-B., Contributed to Investigation, Formal analysis, other contributions. J.M.-T., Contributed to Conceptualization, Supervision, Methodology, Formal analysis, other contributions. A.M.-O., L.A.M.-P., and O.Q.-H., contributed to Conceptualization, Methodology, Supervision, and other contributions. F.A.-C., Formal analysis. R.A.G.-L., Contributed to Conceptualization, Supervision, Methodology, Formal analysis, Writing—original draft, Writing—review & editing. All authors have read and agreed to the published version of the manuscript.

Funding: This work was supported by the research grants 20254008 of the Instituto Politécnico Nacional of Mexico and 158-08-045 of the Universidad Francisco de Paula Santander Ocaña.

Institutional Review Board Statement: Not applicable.

Informed Consent Statement: Not applicable.

Data Availability Statement: The datasets generated and analyzed during the current study are not publicly available due to institutional restrictions, but are available from the corresponding authors upon reasonable request.

Conflicts of Interest: The authors declare that they have no known competing financial interests or personal relationships that could have appeared to influence the work reported in this paper.

Nomenclature

γ	superficial tension
l	penetration length
r	capillary radius
θ	contact angle
μ	dynamic viscosity
t	time
α	angle of inclination of the plane
r_0	initial capillary radius
r_s	imbibition front
ϕ	volumetric flow rate
D	thickness of porous media
K	permeability
P	pressure
v	imbibition front speed
ρ	density
g	gravitational potential
A	cross-sectional area
v_r	instantaneous flow velocity
t_c	critical time

References

1. de Gennes, P.-G.; Brochard-Wyart, F.; Quéré, D. Capillarity: Deformable Interfaces BT—Capillarity and Wetting Phenomena: Drops, Bubbles, Pearls, Waves. In *Capillarity and Wetting Phenomena*; Springer: Berlin/Heidelberg, Germany, 2004.
2. Morrow, N.R.; Mason, G. Recovery of oil by spontaneous imbibition. *Curr. Opin. Colloid Interface Sci.* **2001**, *6*, 321–337. [CrossRef]
3. Washburn, E.W. The dynamics of capillary flow. *Phys. Rev.* **1921**, *17*, 273. [CrossRef]
4. Salam, A.; Wang, X. An analytical solution on spontaneous imbibition coupled with fractal roughness, slippage and gravity effects in low permeability reservoir. *J. Pet. Sci. Eng.* **2022**, *208*, 109501. [CrossRef]
5. Fries, N.; Dreyer, M. An analytic solution of capillary rise restrained by gravity. *J. Colloid Interface Sci.* **2008**, *320*, 259–263. [CrossRef]
6. Cai, J.; Yu, B. A Discussion of the Effect of Tortuosity on the Capillary Imbibition in Porous Media. *Transp. Porous Media* **2011**, *89*, 251–263. [CrossRef]
7. Chang, S.; Kim, W. Dynamics of water imbibition through paper with swelling. *J. Fluid Mech.* **2020**, *892*, A39. [CrossRef]
8. Patari, S.; Mahapatra, P.S. Liquid wicking in a paper strip: An experimental and numerical study. *ACS Omega* **2020**, *5*, 22931–22939. [CrossRef] [PubMed]
9. Cummins, B.M.; Chinthapatla, R.; Ligler, F.S.; Walker, G.M. Time-Dependent Model for Fluid Flow in Porous Materials with Multiple Pore Sizes. *Anal. Chem.* **2017**, *89*, 4377–4381. [CrossRef]
10. Chang, S.; Seo, J.; Hong, S.; Lee, D.G.; Kim, W. Dynamics of liquid imbibition through paper with intra-fibre pores. *J. Fluid Mech.* **2018**, *845*, 36–50. [CrossRef]
11. El-Amin, M.F.; Sun, S. Effects of gravity and inlet/outlet location on a two-phase cocurrent imbibition in porous media. *J. Appl. Math.* **2011**, *2011*, 673523. [CrossRef]
12. Chen, T.; Sun, C.; Abbas, S.C.; Alam, N.; Qiang, S.; Tian, X.; Fu, C.; Zhang, H.; Xia, Y.; Liu, L.; et al. Multi-dimensional microfluidic paper-based analytical devices (μPADs) for noninvasive testing: A review of structural design and applications. *Anal. Chim. Acta* **2024**, *1321*, 342877. [CrossRef]

13. Gharagozlou, A.; Pourjafar-chelikdani, M.; Sadeghy, K. Yield-stress effects on spontaneous imbibition in paper-based kits. *J. Nonnewton. Fluid Mech.* **2024**, *333*, 105326. [CrossRef]
14. Shah, S.B.A. Thermo-mechanical response of Sakesar limestone under cyclic steam injection: Insights from the Potwar Basin, Pakistan. *Phys. Chem. Earth* **2026**, *142*, 104285. [CrossRef]
15. Han, B.; Gao, H.; Xiao, Y.; Ma, Z.; Cheng, Z.; Li, T.; Wang, C.; Luo, K.; Li, X. CO_2 foam-assisted fracturing fluid flowback and CO_2 sequestration in tight sandstone gas reservoirs: Experimental and numerical study. *Geoenergy Sci. Eng.* **2026**, *257*, 214199. [CrossRef]
16. Madhumaya, A.; Maiti, S.; Kulkarni, S.D.; Vyas, A. Forecasting Oil Recovery Under Polymer Enhanced Oil Recovery Technique Using Machine Learning. *Results Eng.* **2026**, *29*, 109216. [CrossRef]
17. Medina, A.; Miranda, J.; Agraz, R.D.; López-villa, A. Radial imbibition in tilted paper sheets. In *Memorias de Divulgación Científica, Tecnológica e Innovación de la SOMIM*; Instituto Tecnológico de Sonora (ITSON): Querétaro, Mexico, 2024.
18. Handy, L.L. Determination of Effective Capillary Pressures for Porous Media from Imbibition Data. *Trans. AIME* **1960**, *219*, 75–80. [CrossRef]
19. Lundblad, A.; Bergman, B.; Soc, J.E.; Lundblad, A.; Bergmant, B. Determination of Contact Angle in Porous Molten-Carbonate Fuel-Cell Electrodes. *J. Electrochem.* **1997**, *144*, 984–987. [CrossRef]
20. Benavente, D.; Lock, P.; Ángeles, M.; Del, G. Predicting the Capillary Imbibition of Porous Rocks from Microstructure. *Transp. Porous Media* **2002**, *49*, 59–76. [CrossRef]
21. Li, K.; Horne, R.N.; Stanford, U. Characterization of Spontaneous Water Imbibition Into Gas-Saturated Rocks. In Proceedings of the SPE/AAPG Western Regional Meeting, Long Beach, CA, USA, 19–22 June 2000; pp. 375–384.
22. Huber, P.; Gr, S. Rheology of liquids in nanopores: A study on the capillary rise of water, *n*-Hexadecane and *n*-Tetracosane in mesoporous silica. *Eur. Phys. J. Spec. Top.* **2007**, *105*, 101–105. [CrossRef]
23. Bejan, A. Convection in Porous Media. In *Convection Heat Transfer*; Springer: Berlin/Heidelberg, Germany, 2013.
24. Richards, L.A. Capillary Conduction of Liquids through porous mediums. *Physics* **1931**, *1*, 318–333. [CrossRef]
25. Balankin, A.S.; Paredes, R.G.; Susarrey, O.; Morales, D.; Vacio, F.C. Kinetic roughening and pinning of two coupled interfaces in disordered media. *Phys. Rev. Lett.* **2006**, *96*, 1–4. [CrossRef] [PubMed]
26. Horvath, V.K.; Stanley, H.E. Temporal scaling of interfaces propagating in porous media. *Phys. Rev. E* **1995**, *52*, 5166. [CrossRef] [PubMed]
27. Lam, C.H.; Horváth, V.K. Pipe network model for scaling of dynamic interfaces in porous media. *Phys. Rev. Lett.* **2000**, *85*, 1238–1241. [CrossRef] [PubMed]

Disclaimer/Publisher's Note: The statements, opinions and data contained in all publications are solely those of the individual author(s) and contributor(s) and not of MDPI and/or the editor(s). MDPI and/or the editor(s) disclaim responsibility for any injury to people or property resulting from any ideas, methods, instructions or products referred to in the content.